

Directed delivery of terahertz frequency radiation from quantum cascade lasers within a dry 3He dilution refrigerator

Cite as: Rev. Sci. Instrum. **93**, 113906 (2022); <https://doi.org/10.1063/5.0102553>

Submitted: 10 June 2022 • Accepted: 08 October 2022 • Published Online: 10 November 2022

Published open access through an agreement with JISC Collections

 M. Vaughan,  W. Michailow, M. Salih, et al.



View Online



Export Citation



CrossMark

ARTICLES YOU MAY BE INTERESTED IN

[A high-throughput catalyst synthesis system for Ag-based catalysts](#)

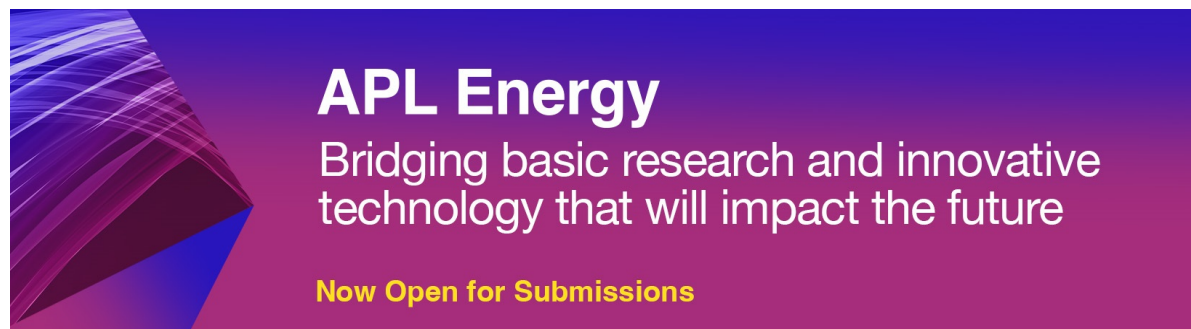
Review of Scientific Instruments **93**, 114101 (2022); <https://doi.org/10.1063/5.0104325>

[Psychological stress recognition from heart rate variability parameters based on field programmable gate arrays](#)

Review of Scientific Instruments **93**, 115107 (2022); <https://doi.org/10.1063/5.0118630>

[HP-TACO: A high-pressure triaxial compression apparatus for in situ x-ray measurements in geomaterials](#)

Review of Scientific Instruments **93**, 113907 (2022); <https://doi.org/10.1063/5.0102931>



APL Energy
Bridging basic research and innovative
technology that will impact the future
Now Open for Submissions

Directed delivery of terahertz frequency radiation from quantum cascade lasers within a dry ^3He dilution refrigerator

Cite as: Rev. Sci. Instrum. 93, 113906 (2022); doi: 10.1063/5.0102553

Submitted: 10 June 2022 • Accepted: 8 October 2022 •

Published Online: 10 November 2022



View Online



Export Citation



CrossMark

M. Vaughan,¹  W. Michailow,²  M. Salih,¹ L. Li,¹  H. Beere,² D. A. Ritchie,²  E. H. Linfield,¹ A. G. Davies,¹ and J. E. Cunningham^{1,a)} 

AFFILIATIONS

¹School of Electronic and Electrical Engineering, University of Leeds, Leeds, West Yorkshire LS2 9JT, United Kingdom

²Cavendish Laboratory, University of Cambridge, Cambridge, Cambridgeshire CB3 0HE, United Kingdom

^{a)}Author to whom correspondence should be addressed: J.E.Cunningham@leeds.ac.uk

ABSTRACT

We present a scheme for the full integration of terahertz (THz) frequency quantum cascade lasers (QCLs) within a dilution refrigerator in order to provide a directed delivery of THz power into the sample space. We describe a successful operation of a 2.68 THz QCL located on the pulse tube cooler stage of the refrigerator, with its output coupled onto a two-dimensional electron gas (2DEG) located on a millikelvin sample stage via hollow metal waveguides and Hysol thermal isolators, achieving a total loss from QCL to the sample of ~ -9 dB. The thermal isolators limit heat leaks to the sample space, with a base temperature of ~ 210 mK being achieved. We observe cyclotron resonance (CR) induced in the 2DEG by the QCL and explore the heating impact of the QCL on all stages of the refrigerator. The CR effect induced by the THz QCL is observable at electron temperatures as low as ~ 430 mK. The results show a viable route for the exploitation of THz QCLs within the environment of a dilution refrigerator and for the THz power delivery in very low-temperature (< 0.5 K) condensed matter experiments.

© 2022 Author(s). All article content, except where otherwise noted, is licensed under a Creative Commons Attribution (CC BY) license (<http://creativecommons.org/licenses/by/4.0/>). <https://doi.org/10.1063/5.0102553>

I. INTRODUCTION

Many condensed matter systems of topical interest have energy gaps or excitations that can be accessed by terahertz (THz) radiation, including the surface states in topological materials,^{1,2} oscillations of spin currents in antiferromagnets,³ and cyclotron absorption in low-dimensional systems.^{4,5} Often, such states are more easily studied or are even only observable at very low temperatures. Quantum cascade lasers (QCLs) can offer a highly stable, relatively high power source of THz radiation⁶ but produce too much waste heat during operation (of order watts) to be directly located within the sample space of any existing dilution refrigerator, which typically offer only microwatts of cooling power at their lowest temperature stages.

In previous work on the THz power delivery from QCLs to low temperature experiments, the QCL has typically been operated outside of the sample refrigerator, within its own cryostat, with

waveguides used to guide THz radiation into the cryostat to the sample space.⁵ Aside from the complexity of then needing to run two cryogenic systems concurrently and in close proximity, this arrangement introduces substantial THz losses at the window used for the exit and entry points of each respective refrigerator, both from the issues of alignment and transmission loss through the windows into the vacuum space. In addition, the total length of waveguides is substantial (typically > 1.2 m). Here, we propose a different scheme in which we integrate the THz QCL within the refrigerator itself by locating it on one of the higher cooling power stages. The QCL output is then coupled to the sample space by short sections of multimode copper tube hollow metal waveguides (HMWGs),⁷ thermally isolated from each other via spacer sections machined from cast epoxy resin HysolTM⁸ (a vacuum- and cryogenic-compatible epoxy with a low thermal conductivity). Given the well-known high losses from most waveguides for THz frequency signals, our technique seeks to trade off the increase in base temperature caused by

the heat load introduced by the QCL mounted within the refrigerator against the need for only a small length of lossy waveguides. Although our HMWG sections are lossy compared with alternative THz waveguides proposed for room temperature operation,^{9,10} they are easily fabricated, robust to cryogenic cycling, and easier to heat sink.

II. CHARACTERIZATION OF COMPONENTS FOR THZ COUPLING

Our HMWG sections were cut from a spool of copper (grade C106) pipe of 4.6 mm internal diameter, straightened, and cut to length using a pipe cutter. Bends and saddle bends (s-bends) were fabricated using a bespoke (3D printed) forming tool to bend the pipe carefully without significantly altering its cross section and with larger radii than normal pipe bending tools allow. The ends of each HMWG section were deburred, leaving a small chamfer. The Hysol thermal isolators [Fig. 1(b)] were fitted over the HMWG with a 2 mm spacing ring to separate the HMWG ends while keeping them aligned. 1/4 in. Wade brass compression fittings were used to support the HMWG [Fig. 1(c)] and only tightened sufficiently to prevent slippage while avoiding deformation to the inside cross section of the HMWG.

A 2.68 THz bound-to-continuum QCL, employing a surface-plasmon waveguide for mode confinement, was patterned

into a laser ridge 2.5 mm long and 200 μm wide. It was attached to a 0.5 mm thick copper block coated with gold and mounted with melted indium. Finally, the contacts of the QCL were ball wire bonded using gold wire to ceramic-insulated contact pads. To characterize the HMWG sections, the QCL was first mounted on a copper cold-finger of a Janis ST-100 cryostat cooled with liquid He to 20 K. The QCL was initially characterized in a pulsed mode using double-modulation technique outside the dilution refrigerator with a 0.8 A current pulse train of 10 kHz repetition rate and 2% duty cycle (for fast modulation), which was electrically gated by a 167 Hz, 50% duty cycle square-wave signal (for slow modulation). The power-current-voltage (LIV) characteristics of the QCL were measured using a He-cooled silicon bolometer (QMC instruments TK1813) that was calibrated using a Thomas Keating 1840 absolute powermeter. The QCL had a peak power of ~ 27.5 mW at 5 K and 22 mW at 50 K.

Losses introduced by the HMWG sections were then measured at room temperature on an optical bench using a pyrometer mounted on a motorized x-y stage for scanning to aid alignment of the QCL facet with the waveguide (Fig. 2). Straight HMWG sections of lengths 10, 20, 30, and 100 cm were used to quantify the waveguide loss and the coupling losses resulting from the cryostat window and the coupling into the waveguide (noting that the window losses were later eliminated when the QCL was mounted inside the dilution refrigerator). Again, in these measurements, the lock-in reference for the pyrometer was derived from the same slow modulation gating frequency of the QCL.

Table I shows the individual component losses from the brass couplings, thermal isolators, and S-bends. Each was measured on the bench by installing it in a short 10 cm section of HMWG and then measuring the increased loss using the same method as before.

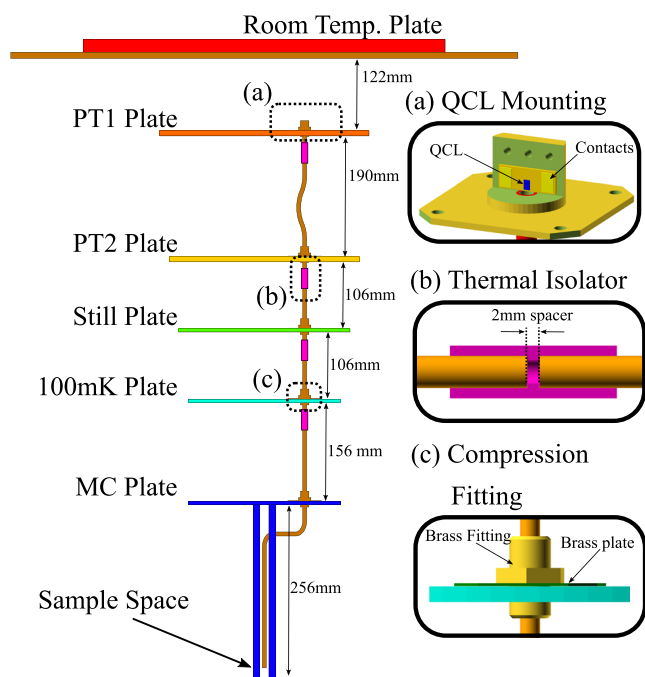


FIG. 1. Arrangement inside the 3He dilution refrigerator with magnified sections (a)–(c). The QCL (a) is located on the PT1 plate and coupled into the sample space via Cu HMWG. PT1 and PT2 are the first and second pulsed tube cooling stages, respectively. MC is the mixing chamber. Each HMWG section is thermally isolated (b) from the next by using Hysol thermal isolators. An S-bend in the waveguide was used to block line-of-sight IR transmission between the PT stages, while compression fittings mechanically support the HMWG (c).

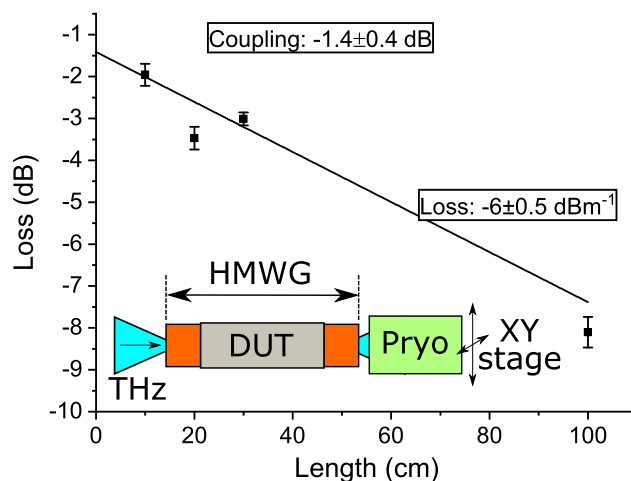


FIG. 2. The HMWG loss as a function of waveguide length normalized to the direct coupling loss between the QCL and the pyrometer. The inset shows the measurement arrangement, with the device under test (DUT) being either more HMWG or one of the components below (Table I). The slope returns a loss rate of -6 ± 0.5 dBm⁻¹, with the y intercept indicating a coupling loss into the waveguide of -1.4 ± 0.4 dB.

TABLE I. Additional loss from each component of the integrated HWMG system.

Component	Loss (dB)
Thermal isolator	-0.88 ± 0.04
Brass fitting	-0.10 ± 0.02
S-bends	-0.8 ± 0.04

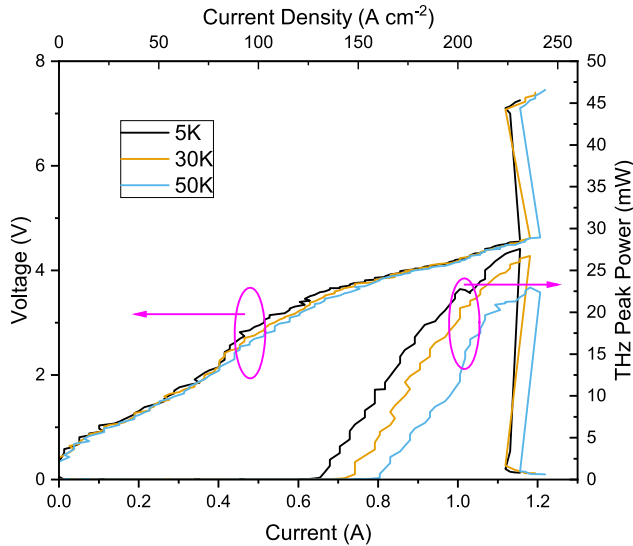


FIG. 3. QCL LIV at different temperatures using a bolometer as a detector. The LIV is showing that the avalanche region is at around ≈ 1200 mA, where lasing stops owing to band misalignment. The right axis shows the QCL peak power. The absolute peak power was measured using a Thomas Keating powermeter.

III. HOLLOW METAL WAVEGUIDE (HWMG) INTEGRATION

We employed a dry Oxford Instrument dilution refrigerator (model Triton DR200), which has three main stages of cooling. The first two stages, PT1 and PT2, employ pulse tube coolers, reaching ~ 47 and 4 K, respectively. Both stages showed slight temperature (± 1 K) variation over time, and between experimental runs, depending on the ambient He compressor pressure (and, therefore, on

room temperature). The final stage is a He^3/He^4 mixing unit able to achieve temperatures below 100 mK.

Each section of HWMG was mechanically supported and thermally coupled to each brass stage using brass compression fittings (Fig. 1(c)). Cryostat stages were thermally decoupled from the HWMG and each other, using Hysol spacers, allowing for a 2 mm gap between each HWMG section. There was sufficient vertical space between the PT1 and PT2 plates to incorporate an s-bend, intended to prevent a direct line-of-sight optical path between the warmer PT1 and the coldest temperature stages.

With all waveguide segments installed, the base temperature of the sample space increased from ~ 99.6 to ~ 206 mK, and the mixing plate temperature increased from ~ 33.3 to ~ 58.3 mK (Table II).

IV. QCL OPERATION INSIDE THE DILUTION REFRIGERATOR

The QCL was next mounted inside the refrigerator on the PT1 plate [Fig. 1(a)] where the cooling power is greatest (~ 40 W specified in manufacturer's data). Alignment of the QCL output into the HWMG was achieved by eye, a result of the large internal diameter of the HWMG (4.6 mm) compared to the QCL ridge structure (200 μm) and the design of the QCL mounting system, which allowed one to be placed directly in front of the other [Fig. 1(a)]. A small amount of Apiezon N grease was applied to improve the thermal conductivity between the QCL and the PT1 plate. A substantial portion of this cooling is needed to remove heat from the lower stages, so we ensured the QCL waste heat was < 2 W. The QCL operated at ~ 47 K (measured using the PT1 thermometer) and powered by an Arroyo 4302 laser power supply in the pulsed mode. To limit heating of the sample-space and PT2 stage, the QCL duty cycle was first set at 5% at a current of 900 mA. The maximum frequency allowed by the Arroyo was 1000 Hz, and so only a simple single modulation mode was used to modulate the QCLs when inside the dilution refrigerator. With this configuration, the sample temperature increased to 268 mK without an applied magnetic field and to 364 mK while sweeping the magnetic field at 0.1 T/min (owing to Eddy current heating) (Table II).

We first investigated the effect of QCL current on refrigerator temperature. For this, the QCL current was increased up to 1300 mA. The stages that showed significant temperature increases were the PT1 stage, mixing chamber, and sample space (Table II). Crucially, at 1300 mA, corresponding to the point where the QCL

TABLE II. Temperature at the key dilution refrigerator stages with and without HWMG, during magnetic field sweeps (with HWMG *in situ*), and during operation of THz QCL (with and without magnetic field sweep). See Fig. 1 for stage positions.

Stage	No HWMG (K)	With HWMG (K)	Sweeping B 0.1 T/min (K)	QCL 900 mA (K)	QCL 1300 mA (K)	QCL 900 mA + B 0.1 T/min (K)	QCL 870 mA + B 0.1 T/min (K)
PT1	46.2	46.7	46.6	46.8	47.0	46.8	47.7
PT2	4.10	3.94	4.14	3.99	3.99	4.17	4.06
Still	0.835	1.009	1.029	1.017	1.020	1.030	1.020
100 mK	0.842	0.846	0.849	0.851	0.854	0.856	0.855
Mixing chamber	0.0333	0.0583	0.0639	0.0689	0.0634	0.0803	0.0640
Sample space	0.099	0.206	0.286	0.268	0.219	0.364	0.308

emission ceases, the mixing chamber and sample space temperature returned to close to base temperature. We can, therefore, conclude that the THz radiation emitted by the QCL is predominantly responsible for the residual heat increase in the mixing chamber and sample space, rather than the dissipation of electrical power in the QCL.

To measure the loss introduced by the HMWG and QCL, we calibrate the sample space thermometer with a known heat load applied to a two-dimensional electron gas (2DEG) sample (discussed later). This was accomplished by using successively larger currents of up to 200 μA through a 1240 Ω sample connection, generating a known value of Joule heating up to 49.6 μW . Under these conditions, the sample stage temperature increased by up to 93 mK, which equates to a conversion factor of 1.87 mK/ μW . From this, we could conclude that the average THz power at 1200 mA drive current and 5% duty cycle was $\sim 138 \mu\text{W}$ and that the peak THz power received by the sample space during the QCL pulse on-time was $\sim 2.8 \text{ mW}$. From Fig. 3, we estimate that the peak output power from the QCL was $\sim 21 \text{ mW}$, implying that the achieved loss from QCL to sample space was $\sim 9 \text{ dB}$. Considering the 4.6 mm internal diameter of the HMWG, we estimate an associated peak power density of $168 \mu\text{W mm}^{-2}$.

V. CYCLOTRON RESONANCE MEASUREMENTS

To demonstrate the THz power transmission into the sample space, we studied cyclotron resonance (CR) induced by the THz radiation in a 2DEG formed in a quantum well $\text{In}_{0.75}\text{Ga}_{0.25}\text{As}/\text{In}_{0.75}\text{Al}_{0.25}\text{As}/\text{GaAs}$ heterostructure seen previously in the work of Tu *et al.*¹¹ The sample is grown by MBE on a GaAs substrate with an InAlAs buffer layer, and the conducting 2DEG channel is within the layer of $\text{In}_{0.75}\text{Ga}_{0.25}\text{As}$ sandwiched between two layers of low ($1 \times 10^{15} \text{ cm}^{-3}$) and high ($2.3 \times 10^{17} \text{ cm}^{-3}$) Si doped $\text{In}_{0.75}\text{Al}_{0.25}\text{As}$ layers. The sample is capped with additional InAlAs and InGaAs layers, placing the 2DEG at a depth of 117 nm. When the CR frequency $\omega_{\text{CR}} = eB/m_e$ matches the QCL frequency ω_{QCL} , we

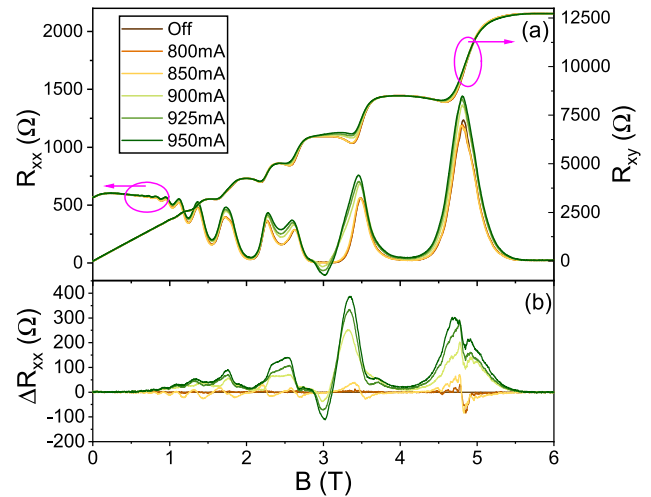


FIG. 5. (a) Sample magnetoresistance as a function of pulsed QCL current, with a QCL pulse frequency of 126 Hz and 5% duty cycle. (b) Difference between each trace of R_{xx} in (a) subtracted from the trace at 0 mA QCL current.

expect a peak in the diagonal resistance.^{12,13} 2DEGs such as these and the CR response are often used to quickly measure effective masses, and that process was used here as a validation tool.

Four terminal electron transport measurements were performed on the 2DEG using two lock-in amplifiers to record the longitudinal and transverse voltages along and across the Hall bar with respect to the direction of current flow. A quasi-constant rms current was set at 100 nA using an applied rms voltage of 0.1 V with a 1 M Ω resistor in series with the sample. The low temperature carrier density and mobility were measured to be $2.84 \times 10^{11} \text{ cm}^{-2}$ and $8.51 \times 10^5 \text{ cm}^2 \text{ V}^{-1} \text{ s}^{-1}$, respectively [Fig. 5(a), R_{xy}]. The effective mass was calculated to be $m^* = (0.03530 \pm 0.0009)m_e$ using the

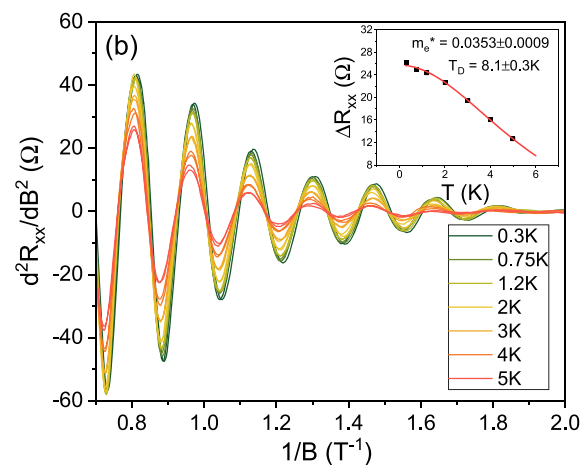
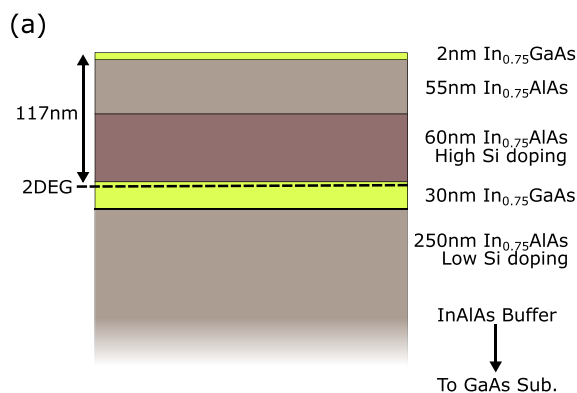


FIG. 4. (a) Simplified layer structure of our $\text{In}_{0.75}\text{Ga}_{0.25}\text{As}/\text{In}_{0.75}\text{Al}_{0.25}\text{As}/\text{GaAs}$ sample; the 2DEG is confined within a quantum well inside the $\text{In}_{0.75}\text{Ga}_{0.25}\text{As}$ layer. (b) Second derivative of the sample longitudinal magnetoresistance as a function of $1/B$ showing SdH oscillations obtained as a function of sample stage temperature. Inset: SdH oscillation amplitude as a function of temperature; a fit to the LK equation yields an effective mass of $0.0353 m_e$ and a Dingle temperature of 8.1 K.

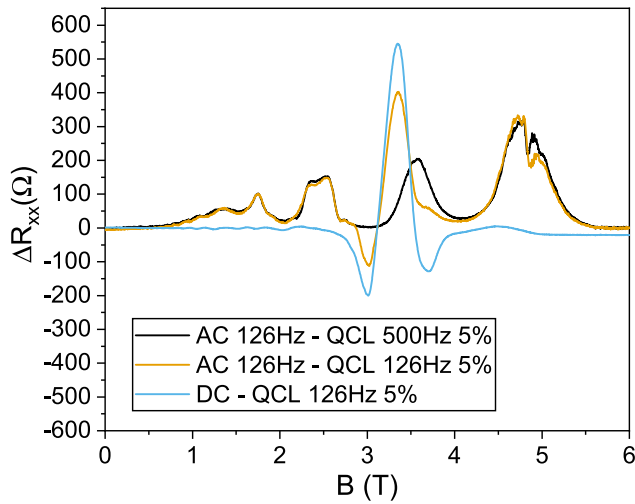


FIG. 6. Three different pulsed QCL 950 mA setups used to isolate the thermal and CR responses as described in the text. The orange trace represents the same 950 mA differential data as shown in Fig. 5(b) for comparison and contains both CR and thermal responses. The black trace filters out CR but keeps the thermal effects. The blue trace filters out thermal effects but keeps the CR response.

Lifshitz–Kosevich (LK) formula [Eq. (1)]¹⁴ and Shubnikov–de Haas (SdH) oscillations in Fig. 4. Using this value, we then expect to see a CR response at 3.38 ± 0.09 T. Figure 5(a) shows the magnetoresistance as a function of B , in which the quantum Hall effect (QHE) was observed, measured in the 2DEG from 0 to 6 T for increasing applied QCL drive currents,

$$\Delta R = 4R_0 e^{-\beta T_D} \frac{\beta T}{\sinh \beta T}, \quad \text{where } \beta = \frac{2\pi^2 K_B m^*}{\hbar e B}. \quad (1)$$

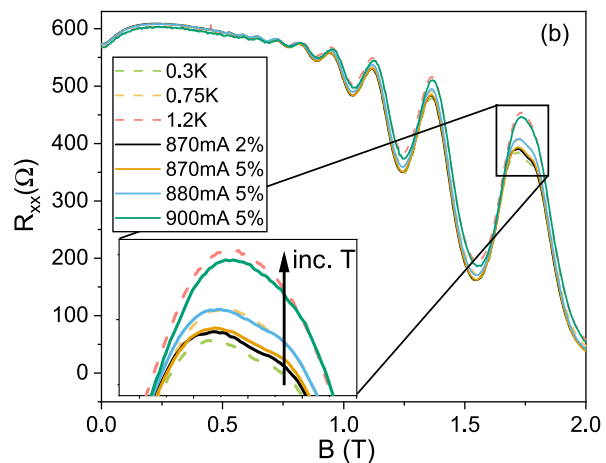
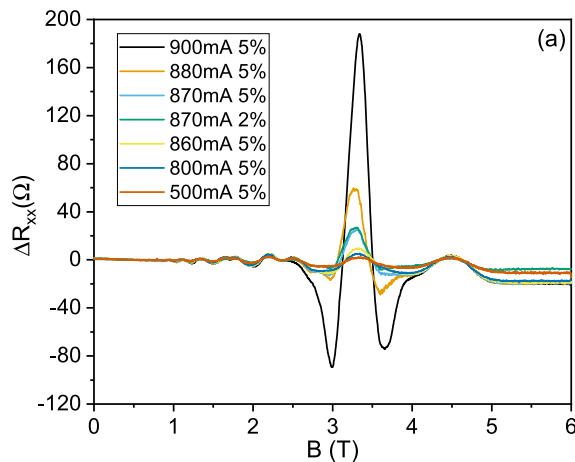


FIG. 7. (a) Low QCL current field sweeps showing a strong CR peak at 3.35 T when above 870 mA, with no clear peak seen below 860 mA. (b) SdH at various sample temperatures (obtained with QCL off) and for different QCL powers and duty cycles. The peak at 1.75 T is found to increase significantly at higher temperatures, which can then be used to estimate the electron temperature as discussed in the text.

Below 850 mA, no response was seen since the QCL was not yet emitting. When the QCL began emitting [at around 870 mA; see Fig. 7(a)], the amplitude of the R_{xx} peaks increased as a result of sample heating, with a negative region found near the expected position for CR. We were able to trigger the pulsed QCL using the same reference as the electrical transport measurement to ensure that the full effect of the QCL was recorded. The difference between QCL off and QCL on is shown in Fig. 5(b). A prominent CR feature is seen at ~ 3.36 T, along with several other peaks, which we ascribe to thermal effects as they replicate the same features (increased FWHM and R_{xx} peak height) as higher temperature QHE measurements.

We can separate the fast CR response from these slower thermal effects by their difference in response time and using the inherent narrow bandpass filtering of the lock-in amplifier. In Fig. 6 (black trace), with a 126 Hz AC electrical measurement and the QCL pulse frequency set at 500 Hz, the lock-in amplifier with its reference frequency set to 126 Hz filters the CR component out but retains the thermal response. Conversely, if we apply a constant DC current to the sample (blue trace) and trigger the QCL pulse at the same frequency as used for the lock-in reference (126 Hz), we keep the CR component but remove the thermal component as seen in the blue trace.

Using this technique, we are left purely with the CR response at 3.338 T, with the other peaks suppressed. This peak position is well within the expected range previously calculated to be 3.38 ± 0.09 T from the LK formula and QCL frequency. The origin for the negative portion either side of the peak is unclear, and we suspect it to be an artifact of the lock-in amplifier anti-aliasing filter, which creates slight distortion from our QCL pulsed square waveform. A similar feature is also seen in the work of Desrat *et al.*¹² although no details on their transport method were given.

For higher values of the QCL drive current, we found that the sample electron temperature could increase substantially to well-above that measured by the sample space thermometry probe

(i.e., higher than the temperatures shown in Table II). For example, we estimate from the SdH amplitude [Fig. 5(a)] that when the QCL was operating at 900 mA and 5% duty cycle, the 2DEG electron temperature increases to ~ 1.2 K. By decreasing the QCL current and/or duty cycle, we achieved substantially lower electron temperatures, however, while maintaining detection of the CR response.

To explore this, Fig. 7(a) shows the 2DES magnetoresistance obtained under QCL illumination for the lowest QCL drive currents. For drive currents higher than 870 mA, there is a clear CR peak, but below this current, the peak is less well defined compared to the residual thermal response, while no discernible CR response is found for QCL currents at 800 and 500 mA. We estimated the electron temperature using the 2DES SdH amplitude (Fig. 4). The SdH peak at 1.74 T was chosen as this region shows a large change with temperature [Fig. 7(b), inset]. We estimate that for the QCL operating at 880 mA and at a 5% duty cycle, 870 mA and 5%, and 870 mA and 2%, the electron temperatures were 0.73, 0.44, and 0.43 K, respectively.

VI. CONCLUSION

We have demonstrated the integration of a THz frequency QCL into a dilution refrigerator and used it to illuminate a mesoscopic 2DEG sample to induce cyclotron resonance. We obtained sample electron temperatures as low as 430 mK under THz irradiation for a suitable choice of QCL emission by controlling the QCL current and pulse duty cycle while observing cyclotron resonance. We anticipate that further improvements to the system, for example, by using tailored QCL designs¹⁵ able to lase at lower currents could yield either even lower temperatures or CW operation of the QCL during dilution refrigeration.

ACKNOWLEDGMENTS

The authors acknowledge funding from the EPSRC HyperTerahertz grant, Grant No. EP/P021859/1. W.M. acknowledges Trinity College Cambridge for a Junior Research Fellowship.

AUTHOR DECLARATIONS

Conflict of Interest

The authors have no conflicts to disclose.

Author Contributions

M. Vaughan: Investigation (equal); Methodology (equal); Writing – original draft (equal); Writing – review & editing (equal). **W. Michailow:** Investigation (equal); Methodology (equal); Resources (equal); Writing – review & editing (equal). **M. Salih:** Resources (equal); Writing – review & editing (equal). **L. Li:** Resources (supporting). **H. Beere:** Resources (equal); Supervision (equal). **D. A. Ritchie:** Resources (supporting); Supervision (equal). **E. H. Linfield:** Supervision (equal). **A. G. Davies:** Project administration (equal); Supervision (equal). **J. E. Cunningham:**

Methodology (equal); Supervision (equal); Writing – original draft (equal); Writing – review & editing (equal).

DATA AVAILABILITY

The data that support the findings of this study are openly available in the University of Leeds data repository.¹⁶

REFERENCES

- X. Chen *et al.*, “Generation and manipulation of chiral terahertz waves in iron-topological insulator heterostructures,” in *International Conference on Infrared, Millimeter, and Terahertz Waves (IRMMW-THz)* (IEEE, 2020), pp. 410–411.
- C. M. Tu, T. T. Yeh, W. Y. Tzeng, Y. R. Chen, H. J. Chen, S. A. Ku, C. W. Luo, J. Y. Lin, K. H. Wu, J. Y. Juang, T. Kobayashi, C. M. Cheng, K. D. Tsuei, H. Berger, R. Sankar, and F. C. Chou, “Manifestation of a second Dirac surface state and bulk bands in THz radiation from topological insulators,” *Sci. Rep.* **5**, 14128 (2015).
- R. Khymyn, I. Lisenkov, V. Tiberkevich, B. A. Ivanov, and A. Slavin, “Antiferromagnetic THz frequency Josephson-like oscillator driven by spin current,” *Sci. Rep.* **7**(1), 43705 (2017); [arXiv:1609.09866](https://arxiv.org/abs/1609.09866).
- Y. Kawano, “Contemporary physics terahertz waves: A tool for condensed matter, the life sciences and astronomy terahertz waves: A tool for condensed matter, the life sciences and astronomy,” *Contemp. Phys.* **54**, 143–165 (2013).
- D. C. Larrabee, G. A. Khodaparast, F. K. Tittel, J. Kono, G. Scalari, L. Ajili, J. Faist, H. Beere, G. Davies, E. Linfield, D. Ritchie, Y. Nakajima, M. Nakai, S. Sasa, M. Inoue, S. Chung, and M. B. Santos, “Application of terahertz quantum-cascade lasers to semiconductor cyclotron resonance,” *Opt. Lett.* **29**, 122 (2004).
- L. H. Li, L. Chen, J. R. Freeman, M. Salih, P. Dean, A. G. Davies, and E. H. Linfield, “Multi-watt high-power THz frequency quantum cascade lasers,” *Electron. Lett.* **53**(12), 799–800 (2017).
- R. Wallis, R. D. Innocenti, D. S. Jessop, O. Mitrofanov, C. M. Bledt, J. E. Melzer, J. A. Harrington, H. E. Beere, and D. A. Ritchie, “Investigation of hollow cylindrical metal terahertz waveguides suitable for cryogenic environments,” *Opt. Express* **24**, 30002 (2016).
- Hysol polyurethane epoxy, type IV, The Dexter Corporation, Olean, NY.
- B. Bowden, J. A. Harrington, and O. Mitrofanov, “Silver/polystyrene coated hollow glass waveguides for the transmission of THz radiation,” *Opt. Lett.* **32**, 2945–2947 (2007).
- Y. Matsuura and E. Takeda, “Hollow optical fibers loaded with an inner dielectric film for terahertz broadband spectroscopy,” *J. Opt. Soc. Am. B* **25**, 1949 (2008).
- C. Chen, I. Farrer, S. N. Holmes, F. Sfigakis, M. P. Fletcher, H. E. Beere, and D. A. Ritchie, “Growth variations and scattering mechanisms in metamorphic $\text{In}_{0.75}\text{Ga}_{0.25}\text{As}/\text{In}_{0.75}\text{Al}_{0.25}\text{As}$ quantum wells grown by molecular beam epitaxy,” *J. Crystal Growth* **425**, 70–75 (2015).
- W. Desrat, F. Giazotto, V. Pellegrini, F. Beltram, F. Capotondi, G. Biasiol, L. Sorba, and D. K. Aude, “Magnetotransport in high-g-factor low-density two-dimensional electron systems confined in $\text{In}_{0.75}\text{Ga}_{0.25}\text{As}/\text{In}_{0.75}\text{Al}_{0.25}\text{As}$ quantum wells,” *Phys. Rev. B* **69**, 245324 (2004); [arXiv:0401325](https://arxiv.org/abs/0401325) [cond-mat].
- A. V. Ikonnikov, K. V. Maremyanin, S. V. Morozov, V. I. Gavrilenko, A. Y. Pavlov, N. V. Shchavruk, R. A. Khabibullin, R. R. Reznik, G. E. Cirlin, F. I. Zubov, A. E. Zhukov, and Z. I. Alferov, “Terahertz radiation generation in multilayer quantum-cascade heterostructures,” *Tech. Phys. Lett.* **43**, 362–365 (2017).
- D. Shoenberg, *Magnetic Oscillations in Metals* (Cambridge University Press, 1984), <https://www.cambridge.org/core/books/magnetic-oscillations-in-metals/56C41223B4CDE32E43BD3109BFD74722>.
- M. Razeghi, S. Slivken, Y. Bai, B. Gokden, and S. R. Darvish, “High power quantum cascade lasers,” *New J. Phys.* **11**, 125017 (2009).
- M. Vaughan, W. Michailow, M. Salih, L. Li, H. Beere, D. A. Ritchie, E. Linfield, A. G. Davies, and J. Cunningham (2022). “Dataset associated with ‘Directed delivery of terahertz frequency radiation within a dry 3He dilution refrigerator,’” University of Leeds, Dataset <https://doi.org/10.5518/1164>.